

## Electrostatic Screening of Charged Defects in Monolayer MoS<sub>2</sub>

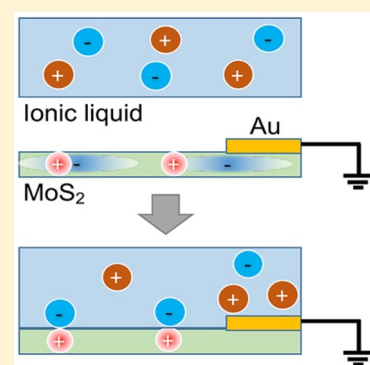
T. L. Atallah,<sup>†</sup> J. Wang,<sup>†</sup> M. Bosch,<sup>†</sup> D. Seo,<sup>‡</sup> R. A. Burke,<sup>§</sup> O. Moneer,<sup>†</sup> Justin Zhu,<sup>†</sup> M. Theibault,<sup>†</sup> L. E. Brus,<sup>†</sup> J. Hone,<sup>‡</sup> and X.-Y. Zhu<sup>\*,†</sup>

<sup>†</sup>Department of Chemistry, Columbia University, New York, New York 10027, United States

<sup>‡</sup>Department of Mechanical Engineering, Columbia University, New York, New York 10027, United States

<sup>§</sup>Sensors and Electron Devices Directorate, US Army Research Laboratory, Adelphi, Maryland 20783, United States

**ABSTRACT:** Defects in monolayer transition-metal dichalcogenides (TMDCs) may lead to unintentional doping, charge-carrier trapping, and nonradiative recombination. These effects impair electronic and optoelectronic technologies. Here we show that charged defects in MoS<sub>2</sub> monolayers can be effectively screened when they are in contact with an ionic liquid (IL), leading to an increase in photoluminescence (PL) yield by up to two orders of magnitude. The extent of this PL enhancement by the IL correlates with the brightness of each pretreated sample. We propose the existence of two classes of nonradiative recombination centers in monolayer MoS<sub>2</sub>: (i) charged defects that relate to unintentional doping and may be electrostatically screened by ILs and (ii) neutral defects that remain unaffected by the presence of ILs.



Monolayer transition-metal dichalcogenides (TMDCs)<sup>1,2</sup> show promise as model systems for 2D physics and for nanoscale electronic, optoelectronic, and photonic devices.<sup>3–9</sup> However, the prevalence of defects<sup>10–12</sup> that serve as uncontrolled dopants, charge-carrier traps, and nonradiative recombination centers stand as a major barrier to studying intrinsic 2D physics and for the realization of efficient monolayer devices.<sup>13–16</sup> While optimizing the growth process of 2D materials reduces atomic defects, other defects may form as a result of exfoliation, device fabrication, and chemical/thermal damage. Furthermore, a monolayer TMDC effectively functions as an interface making its electronic properties highly sensitive to its local environment, such as chemical, topological, and electrostatic inhomogeneity on the supporting substrate surface. Several strategies have been employed to mitigate or reduce traps in TMDC monolayers, including superacid treatments,<sup>17–19</sup> molecular oxygen adsorption,<sup>20</sup> substrate selection<sup>21</sup> or passivation,<sup>22</sup> and encapsulation in hexagonal boron nitride.<sup>22–24</sup> Here we demonstrate a simple and reversible approach to reduce nonradiative trap centers in monolayer MoS<sub>2</sub>. We find that charged defects in MoS<sub>2</sub> monolayers can be electrostatically passivated by contact with ionic liquids (ILs). ILs are extensively used as gate dielectrics because the high capacitance from the interfacial electric double-layer formation enables very high charge injection densities (>10<sup>14</sup>/cm<sup>2</sup>) at low gating voltages.<sup>25–27</sup> Notably, high-density doping from IL gating has led to the demonstration of superconductivity in TMDCs.<sup>28–30</sup> However, electrostatic interaction also spontaneously occurs between the mobile ions in an IL and charges on a semiconductor surface.<sup>31</sup> Here we show that such interactions can reduce doping and increase photoluminescence (PL) intensity by up to two orders

of magnitude in TMDC monolayers. We interpret these findings as the screening of charged trap sites in the TMDC monolayer by mobile anions in the IL, an effect that is similar to the “healing” of surface defects on organic semiconductors by local polar bonds in perfluoropolyether (PFPE).<sup>32</sup>

The samples used in the present study consist of monolayers of MoS<sub>2</sub> from chemical vapor depositions (CVDs) or exfoliation. Typically, we chose monolayer TMDC flakes with lateral dimensions of ~10 μm either grown or exfoliated onto SiO<sub>2</sub>/Si substrates. Through e-beam lithography we introduced Ti/Al/Au contacts (see optical microscope image in Figure 1a). For larger samples we painted graphite (TED PELLA)

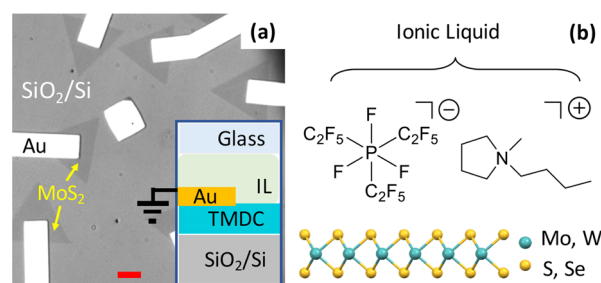


**Figure 1.** (a) Optical microscope image of CVD MoS<sub>2</sub> flakes (dark triangles) with Au metal contacts (bright strips) on a SiO<sub>2</sub>/Si substrate. Scale bar (red): 10 μm. The inset shows schematically the sample after contact with an ionic liquid. (b) Molecular formula of the ionic liquid and atomic model for a TMDC monolayer.

**Received:** March 24, 2017

**Accepted:** April 27, 2017

**Published:** April 27, 2017

electrodes onto the MoS<sub>2</sub> flakes. To form the TMDC/IL interface, we deposited a small drop of an IL on the sample and then covered the sample with a glass coverslip. We performed all PL measurements at room temperature in a dry N<sub>2</sub> atmosphere or in vacuum on a home-built epi-fluorescence microscope, with the excitation light from CW lasers emitting 532 or 514 nm and at power densities of 4 kW/cm<sup>2</sup>. We measured PL far (>1 μm) from the electrodes to avoid quenching by the Au/graphite.

The PL yield from MoS<sub>2</sub> monolayers are known to be low, typically <1%, and vary greatly depending on sample preparation.<sup>1,2,17,21</sup> Figure 2 shows representative PL spectra

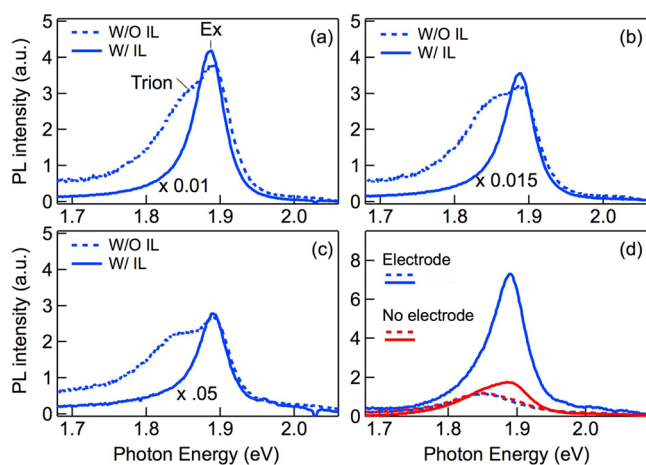


**Figure 2.** Photoluminescence (PL) spectra from MoS<sub>2</sub> monolayers in the absence (dashed) and presence (solid) of an ionic liquid for three different samples (a–c). Note the different scaling factors for the solid curves: (a)  $\times 0.01$ , (b)  $\times 0.015$ , and (c)  $\times 0.05$ . (d) PL spectra from two monolayer MoS<sub>2</sub> flakes on the same sample, one with (blue) and one without (red) Au electrode contact. The dashed and solid curves represent the absence and presence, respectively, of ionic liquids.

(dashed curves) from different monolayer MoS<sub>2</sub> flakes on the SiO<sub>2</sub> surface. We find that the PL intensity from these CVD samples varies by as much as one order of magnitude from sample to sample (dashed curves in Figure 2a–c). Each PL spectrum features a main exciton peak at 1.89 eV and a lower energy shoulder at ~1.85 eV that is attributed to trions.<sup>33</sup> After applying an IL to each monolayer MoS<sub>2</sub> flake, we find that the PL intensity from the exciton peak for each spectrum (solid curves in Figures 2a–c) increases by one to two orders of magnitude, while the trion peak is no longer resolved relative to the dominant exciton peak. Within experimental uncertainty, there is little change to the exciton peak position before and after contact with IL. The removal of electrons from the MoS<sub>2</sub> monolayer has been shown to induce a small red shift in the exciton PL peak,<sup>33</sup> while the increased dielectric screening by IL is expected to induce a blue shift.<sup>34</sup> For the sample in Figure 2d, the apparent “blue” shift with IL simply results from the fact that the lower energy trion emission dominates before IL contact, while the exciton emission dominates after IL.

The PL enhancement effect requires a grounded metal contact to the TMDC monolayer. As shown in Figure 2d for one CVD MoS<sub>2</sub> flake, in the absence of a metal contact, the PL increases only slightly ( $\sim 40\%$ ) upon contact with an IL (red dashed  $\rightarrow$  red solid curve), while the same sample shows an order of magnitude increase in PL intensity when grounded (blue dashed  $\rightarrow$  blue solid curve). As we discuss in detail below,

the necessity of electrical grounding for the enhancement of PL intensity is consistent with the electrostatic screening of charged defects by the high dielectric environment of an IL.

We quantitatively establish the correlation between the enhancement factor ( $\gamma$ ) in PL intensity (by IL) and the brightness of the pre-treated CVD MoS<sub>2</sub> monolayer samples, such as those in Figure 2. Here we define  $\gamma$  as the ratio of the PL intensity in the presence and absence of an IL. Figure 3

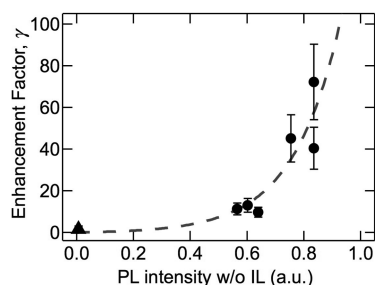


**Figure 3.** Enhancement factor ( $\gamma$ ) in exciton intensity by the presence of an ionic liquid as a function of the original PL intensity ( $I_{\text{ex}}^0$ ) of MoS<sub>2</sub> monolayers. The solid circles are data points and the dashed line is an exponential fit which serves as a guide to the eye.

plots  $\gamma$  versus the total PL intensity in the absence of an IL,  $I_{\text{ex}}^0$ , from the CVD MoS<sub>2</sub> monolayer samples investigated here. The enhancement factor,  $\gamma$ , rises monotonically with  $I_{\text{ex}}^0$ . The data point near the origin (triangle) is the average value of measurements from a dim sample with pretreated PL intensity approximately two orders of magnitude lower than those from the bright samples (circles); the enhancement factor from this dim sample was  $\gamma \approx 1.5$ .

We test the reversibility of the PL enhancement effect by rinsing off and reapplying the IL. As shown in Figure 4, for a

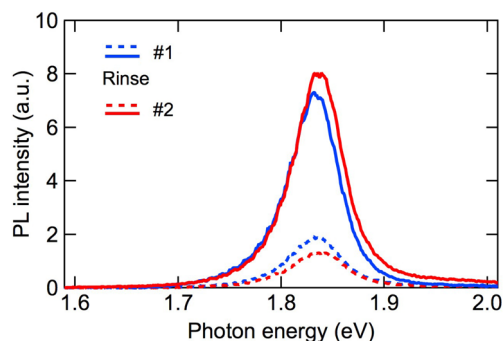


**Figure 4.** Reversible effect of PL enhancement from a CVD MoS<sub>2</sub> monolayer flake with an Au electrode contact. The blue spectra are from MoS<sub>2</sub> monolayers in the absence (dashed) and presence (solid) of an ionic liquid. The red spectra show the PL spectra after removing the IL (dashed) and reapplying the IL (solid).

monolayer MoS<sub>2</sub> flake with Au electrode contact, the PL spectrum (blue dashed curve) initially shows low intensity, then is enhanced by the addition of IL (blue solid curve). The PL intensity is reset to the initial level when we rinse off the IL (red dashed curve) and is enhanced again when we reapply an IL to the MoS<sub>2</sub> monolayer (red solid curve). Within experimental uncertainty ( $\pm 20\%$ ) in PL intensity from measurement to measurement, we conclude that the enhancement of the PL intensity by an IL is reversible.

The observed enhancement of the PL intensity by an IL and the reversibility of this effect suggest an electrostatic origin, distinct from irreversible chemical treatments. Among a number of defects identified in monolayer MoS<sub>2</sub>, the dominant kind is the S-vacancy, which may be related to n-type doping and positively charged sites.<sup>10–12</sup> The latter is shown in Figure 5a as a localized positive charge (red) with a delocalized

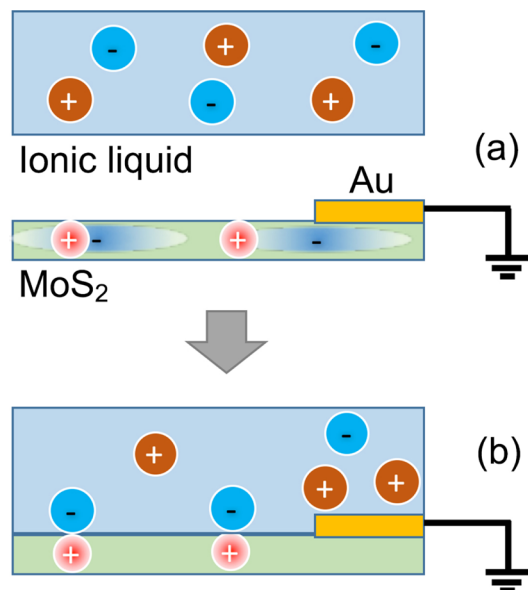


**Figure 5.** Schematic illustration of the electrostatic passivation of positively charged defects in MoS<sub>2</sub> monolayer (green) when it is contacted with an IL (blue). (a) Initially, the grounded MoS<sub>2</sub> monolayer is not in contact with the IL and so has local sulfur vacancies (shown by +), resulting in n-type doping with delocalized electrons (shown by -). (b) After contacting with an IL, the anions screen the positive charge traps and the excess electrons in MoS<sub>2</sub> move to the ground.

electron (blue) in the MoS<sub>2</sub> monolayer (green). Upon treatment, the IL screens the localized charges, as schematically represented by the binding of anions in the IL to the trapped positive charge in MoS<sub>2</sub>. The chemical potential of the electron in the MoS<sub>2</sub> monolayer is increased by such screening, and this leads to a depletion of electrons (i.e., majority carrier from n-type doping) from the conduction band (Figure 5b) into ground. This is consistent with the disappearance of the trion peak in PL spectra after the MoS<sub>2</sub> monolayers contact the IL and the need of electrode contact (Figure 2). Both positively charged and neutral traps located within the bandgap can serve as nonradiative recombination centers via Auger-type of mechanisms, as proposed by Wang et al.<sup>15</sup> The positively charged traps can be reversibly passivated by ILs, leading to the enhancement in PL yield, but the charge-neutral traps cannot. Examples of charge-neutral traps may include antisites and O–S substitutions.<sup>35–38</sup> The coexistence of both neutral and charged traps for nonradiative recombination can explain the observed strong correlation between  $\gamma$  and  $I_{\text{ex}}^{\text{trion}}$ , as seen in Figure 3. The concentrations of both types of traps are likely correlated; that is, both increase with increasing defect density. Because electrostatic passivation by an IL only passivates the charged traps, the enhancement factor correlates inversely with the neutral trap density or total defect density. This is responsible for the positive correlation of  $\gamma$  with  $I_{\text{ex}}^{\text{trion}}$ , Figure 3.

The observed PL enhancement by an IL and the proposed electrostatic passivation mechanism are consistent with previous reports of PL enhancement in MoS<sub>2</sub> monolayer by oxygen adsorption or superacid treatment. Nan et al. reported PL intensity enhancement by as large as 10<sup>3</sup> when defective MoS<sub>2</sub> monolayers were treated with oxygen and suggested that the adsorption of oxygen to S-vacancy sites is responsible.<sup>20</sup> Because the chemisorbed oxygen atoms/molecules should be in a partially reduced state (negatively charged), there can be an electrostatic contribution to the passivation of positively charged traps. Javey and coworkers reported the enhancement in PL efficiency to as large as unity when MoS<sub>2</sub> monolayers were treated with a superacid, bis(trifluoromethane) sulfonimide (TFSI).<sup>17–19</sup> TFSI is a common anion in ILs. We posit that the reduction of TFSI by electrons in the n-type MoS<sub>2</sub> leads to hydrogen (gas) evolution, resulting in TFSI anions that passivate positively charged defects/traps. In fact, several studies show that S-vacancies provide active sites in MoS<sub>2</sub> catalysts to evolve hydrogen gas.<sup>39–41</sup>

In summary, we demonstrate the effective screening and passivation of charged defects in monolayer MoS<sub>2</sub>, leading to an increase in the PL yield by up to two orders of magnitude. We show a correlation between the enhancement of PL yield with the brightness of the MoS<sub>2</sub> monolayer sample and suggest the presence of both charged and neutral nonradiative recombination centers. The former can be passivated by IL but the latter cannot. Electrostatic screening can be used as a means to passivate charged defects as well as to distinguish the nature of nonradiative recombination centers in monolayer TMDCs.

## EXPERIMENTAL METHODS

**MoS<sub>2</sub> Monolayer CVD Growth.**<sup>42</sup> Cleaned Si/SiO<sub>2</sub> substrates were placed at the center of a furnace beside a MoO<sub>3</sub>-covered silicon substrate. ~1 g of sublimated sulfur was placed at the opening of the furnace where the sulfur reached an approximate maximum temperature of 600 °C. The center of the furnace was heated to 550 °C over a period of 30 min (20 °C/min) with a nitrogen flow rate of 200 sccm. The furnace was then heated to 850 °C at a slower pace of ~5 °C/min. After sitting at this temperature for 10–15 min, the furnace was allowed to cool naturally back to room temperature yielding the monolayer MoS<sub>2</sub> triangular flakes. Larger CVD MoS<sub>2</sub> samples were bought from 2D Layer (<http://2dlayer.com>).

**Fabrication of Electrodes.** For smaller samples (<10 μm) electrodes were placed by e-beam lithography with a PMMA resist using a Nanobeam nB4 instrument. Metallic contacts consisting of Ti (3 nm)/Al (20 nm)/Au (50 nm) were deposited using either thermal (home-built deposition system) or e-beam (Angstrom Evovac Deposition System) evaporation at rates of 1 Å/s. For larger flakes, graphite paint (TED PELLA) was applied and flakes that were in contact with the graphite were used. To make electrical contact to the electrodes, gold wire was painted on with graphite paint and held down with Kapton tape.

**Optical Measurements.** We carried out PL measurements using home-built far-field epi-fluorescence microscope setups (Olympus IX73 or Nikon TE300 inverted microscopes). We mounted all samples in either a N<sub>2</sub>-gas-filled cell or evacuated cryostat for optical measurements. The excitation light used was either a 532 nm commercial frequency-doubled YAG laser (MDL-III-532-200 mW) or an argon ion laser operating at 514.5 nm (CVI Melles-Griot). The light was focused onto the sample surface by a 40×, NA 0.60 objective with a correction

collar (Olympus LUCPLFLN40X or Nikon CFISPLFLELWD-40X). The laser spot size was focused to spot size of 0.7  $\mu\text{m}$  diameter. The emission from each monolayer was collected by the same objective and focused into a spectrograph (Princeton Instrument Acton SP2300i with a 300  $\text{mm}^{-1}$  grating or Princeton Instruments Acton 300i with a 150  $\text{mm}^{-1}$  grating) and detected by a CCD camera (charge-coupled device; PyLoN 400 or PI-Photon). The instrument resolution was  $\sim 0.4$  nm. All measurements were carried out at room temperature.

## AUTHOR INFORMATION

### Corresponding Author

\*E-mail: xyzhu@columbia.edu.

### ORCID

X.-Y. Zhu: 0000-0002-2090-8484

### Notes

The authors declare no competing financial interest.

## ACKNOWLEDGMENTS

Sample preparation was carried out in the Center for Precision Assembly of Superstratic and Superatomic Solids supported the National Science Foundation (NSF) grant DMR-1420634. Spectroscopic measurements were supported by the NSF grant DMR 1608437 after September 1, 2016. Before September 1, 2016, the initial spectroscopic measurements were supported by the U.S. Department of Energy, Office of Science, Grant ER46979.

## REFERENCES

- (1) Mak, K.; Lee, C.; Hone, J.; Shan, J.; Heinz, T. Atomically Thin  $\text{MoS}_2$ : A New Direct-Gap Semiconductor. *Phys. Rev. Lett.* **2010**, *105*, 136805.
- (2) Splendiani, A.; Sun, L.; Zhang, Y.; Li, T.; Kim, J.; Chim, C.-Y.; Galli, G.; Wang, F. Emerging Photoluminescence in Monolayer  $\text{MoS}_2$ . *Nano Lett.* **2010**, *10*, 1271–1275.
- (3) Kang, S. J.; Lee, G.-H.; Yu, Y.-J.; Zhao, Y.; Kim, B.; Watanabe, K.; Taniguchi, T.; Hone, J.; Kim, P.; Nuckolls, C. Organic Field Effect Transistors Based on Graphene and Hexagonal Boron Nitride Heterostructures. *Adv. Funct. Mater.* **2014**, *24*, 5157–5163.
- (4) Wang, Q. H.; Kalantar-Zadeh, K.; Kis, A.; Coleman, J. N.; Strano, M. S. Electronics and Optoelectronics of Two-Dimensional Transition Metal Dichalcogenides. *Nat. Nanotechnol.* **2012**, *7*, 699–712.
- (5) Desai, S. B.; Madhvapathy, S. R.; Sachid, A. B.; Llinas, J. P.; Wang, Q.; Ahn, G. H.; Pitner, G.; Kim, M. J.; Bokor, J.; Hu, C.; et al.  $\text{MoS}_2$  Transistors with 1-Nanometer Gate Lengths. *Science* **2016**, *354*, 99–102.
- (6) Liu, X.; Galfsky, T.; Sun, Z.; Xia, F.; Lin, E.; Lee, Y.-H.; Kéna-Cohen, S.; Menon, V. M. Strong Light–matter Coupling in Two-Dimensional Atomic Crystals. *Nat. Photonics* **2014**, *9*, 30–34.
- (7) Xia, F.; Wang, H.; Xiao, D.; Dubey, M.; Ramasubramanian, A. Two-Dimensional Material Nanophotonics. *Nat. Photonics* **2014**, *8*, 899–907.
- (8) Zhang, Y. J.; Oka, T.; Suzuki, R.; Ye, J. T.; Iwasa, Y. Electrically Switchable Chiral Light-Emitting Transistor. *Science* **2014**, *344*, 725–728.
- (9) Xu, X.; Yao, W.; Xiao, D.; Heinz, T. F. Spin and Pseudospins in Layered Transition Metal Dichalcogenides. *Nat. Phys.* **2014**, *10*, 343–350.
- (10) Santosh, K. C.; Longo, R. C.; Addou, R.; Wallace, R. M.; Cho, K. Impact of Intrinsic Atomic Defects on the Electronic Structure of  $\text{MoS}_2$  Monolayers. *Nanotechnology* **2014**, *25*, 375703.
- (11) Zhou, W.; Zou, X.; Najmaei, S.; Liu, Z.; Shi, Y.; Kong, J.; Lou, J.; Ajayan, P. M.; Yakobson, B. I.; Idrobo, J.-C. Intrinsic Structural Defects in Monolayer Molybdenum Disulfide. *Nano Lett.* **2013**, *13*, 2615–2622.
- (12) Vancsó, P.; Magda, G. Z.; Pető, J.; Noh, J.-Y.; Kim, Y.-S.; Hwang, C.; Biró, L. P.; Tapasztó, L. The Intrinsic Defect Structure of Exfoliated  $\text{MoS}_2$  Single Layers Revealed by Scanning Tunneling Microscopy. *Sci. Rep.* **2016**, *6*, 29726.
- (13) Guo, Y.; Wei, X.; Shu, J.; Liu, B.; Yin, J.; Guan, C.; Han, Y.; Gao, S.; Chen, Q. Charge Trapping at the  $\text{MoS}_2$ - $\text{SiO}_2$  Interface and Its Effects on the Characteristics of  $\text{MoS}_2$  Metal-Oxide-Semiconductor Field Effect Transistors. *Appl. Phys. Lett.* **2015**, *106*, 103109.
- (14) Tongay, S.; Suh, J.; Ataca, C.; Fan, W.; Luce, A.; Kang, J. S.; Liu, J.; Ko, C.; Raghunathanan, R.; Zhou, J.; et al. Defects Activated Photoluminescence in Two-Dimensional Semiconductors: Interplay between Bound, Charged, and Free Excitons. *Sci. Rep.* **2013**, *3*, 2657.
- (15) Wang, H.; Zhang, C.; Rana, F. Ultrafast Dynamics of Defect-Assisted Electron-Hole Recombination in Monolayer  $\text{MoS}_2$ . *Nano Lett.* **2015**, *15*, 339–345.
- (16) McDonnell, S.; Addou, R.; Buie, C.; Wallace, R. M.; Hinkle, C. L. Defect-Dominated Doping and Contact Resistance in  $\text{MoS}_2$ . *ACS Nano* **2014**, *8*, 2880–2888.
- (17) Amani, M.; Lien, D.-H.; Kiriya, D.; Xiao, J.; Azcatl, A.; Noh, J.; Madhvapathy, S. R.; Addou, R.; KC, S.; Dubey, M.; Cho, K.; et al. Near-Unity Photoluminescence Quantum Yield in  $\text{MoS}_2$ . *Science* **2015**, *350*, 1065–1068.
- (18) Amani, M.; Addou, R.; Ahn, G. H.; Kiriya, D.; Taheri, P.; Lien, D.-H.; Ager, J. W.; Wallace, R. M.; Javey, A. Recombination Kinetics and Effects of Superacid Treatment in Sulfur and Selenium Based Transition Metal Dichalcogenides. *Nano Lett.* **2016**, *16*, 2786–2791.
- (19) Han, H.-V.; Lu, A.-Y.; Lu, L.-S.; Huang, J.-K.; Li, H.; Hsu, C.-L.; Lin, Y.-C.; Chiu, M.-H.; Suenaga, K.; Chu, C.-W.; et al. Photoluminescence Enhancement and Structure Repairing of Monolayer  $\text{MoSe}_2$  by Hydrohalic Acid Treatment. *ACS Nano* **2016**, *10*, 1454–1461.
- (20) Nan, H.; Wang, Z.; Wang, W.; Liang, Z.; Lu, Y.; Chen, Q.; He, D.; Tan, P.; Miao, F.; Wang, X.; et al. Strong Photoluminescence Enhancement of  $\text{MoS}_2$  through Defect Engineering and Oxygen Bonding. *ACS Nano* **2014**, *8*, 5738–5745.
- (21) Liu, B.; Zhao, W.; Ding, Z.; Verzhbitskiy, I.; Li, L.; Lu, J.; Chen, J.; Eda, G.; Loh, K. P. Engineering Bandgaps of Monolayer  $\text{MoS}_2$  and  $\text{WS}_2$  on Fluoropolymer Substrates by Electrostatically Tuned Many-Body Effects. *Adv. Mater.* **2016**, *28*, 6457–6464.
- (22) Ajayi, O. A.; Ardelean, J. V.; Shepard, G. D. G.; Wang, J.; Antony, A.; Taniguchi, T. T.; Watanabe, K.; Heinz, T. F.; Strauf, S.; Zhu, X. X.-Y.; Hone, J. C. Approaching the Intrinsic Photoluminescence Linewidth in Transition Metal Dichalcogenide Monolayers. *2D Mater.* **2017**, DOI: 10.1088/2053-1583/aa6aa1. In press.
- (23) Cui, X.; Lee, G.-H.; Kim, Y. D.; Arefe, G.; Huang, P. Y.; Lee, C.; Chenet, D. A.; Zhang, X.; Wang, L.; Ye, F.; et al. Multi-Terminal Transport Measurements of  $\text{MoS}_2$  Using a van Der Waals Heterostructure Device Platform. *Nat. Nanotechnol.* **2015**, *10*, 534–540.
- (24) Lee, G.-H.; Cui, X.; Kim, Y. D.; Arefe, G.; Zhang, X.; Lee, C.-H.; Ye, F.; Watanabe, K.; Taniguchi, T.; Kim, P.; et al. Highly Stable, Dual-Gated  $\text{MoS}_2$  Transistors Encapsulated by Hexagonal Boron Nitride with Gate-Controllable Contact, Resistance, and Threshold Voltage. *ACS Nano* **2015**, *9*, 7019–7026.
- (25) Ueno, K.; Nakamura, S.; Shimotani, H.; Ohtomo, A.; Kimura, N.; Nojima, T.; Aoki, H.; Iwasa, Y.; Kawasaki, M. Electric-Field-Induced Superconductivity in an Insulator. *Nat. Mater.* **2008**, *7*, 855–858.
- (26) Cho, J. H.; Lee, J.; Xia, Y.; Kim, B.; He, Y.; Renn, M. J.; Lodge, T. P.; Frisbie, C. D. Printable Ion-Gel Gate Dielectrics for Low-Voltage Polymer Thin-Film Transistors on Plastic. *Nat. Mater.* **2008**, *7*, 900–906.
- (27) Jeong, J.; Aetukuri, N.; Graf, T.; Schladt, T. D.; Samant, M. G.; Parkin, S. S. P. Suppression of Metal-Insulator Transition in  $\text{VO}_2$  by Electric Field-Induced Oxygen Vacancy Formation. *Science* **2013**, *339*, 1402–1405.
- (28) Saito, Y.; Nakamura, Y.; Bahramy, M. S.; Kohama, Y.; Ye, J.; Kasahara, Y.; Nakagawa, Y.; Onga, M.; Tokunaga, M.; Nojima; et al.

Superconductivity Protected by Spin–valley Locking in Ion-Gated MoS<sub>2</sub>. *Nat. Phys.* **2015**, *12*, 144–149.

(29) Costanzo, D.; Jo, S.; Berger, H.; Morpurgo, A. F. Gate-Induced Superconductivity in Atomically Thin MoS<sub>2</sub> Crystals. *Nat. Nanotechnol.* **2016**, *11*, 339–344.

(30) Lu, J. M.; Zheliuk, O.; Leermakers, I.; Yuan, N. F. Q.; Zeitler, U.; Law, K. T.; Ye, J. T. Evidence for Two-Dimensional Ising Superconductivity in Gated MoS<sub>2</sub>. *Science* **2015**, *350*, 1353–1357.

(31) Atallah, T. L.; Gustafsson, M. V.; Schmidt, E.; Frisbie, C. D.; Zhu, X.-Y. Charge Saturation and Intrinsic Doping in Electrolyte-Gated Organic Semiconductors. *J. Phys. Chem. Lett.* **2015**, *6*, 4840–4844.

(32) Lee, B.; Chen, Y.; Fu, D.; Yi, H. T.; Czelen, K.; Najafov, H.; Podzorov, V. Trap Healing and Ultralow-Noise Hall Effect at the Surface of Organic Semiconductors. *Nat. Mater.* **2013**, *12*, 1125–1129.

(33) Mak, K. F.; He, K.; Lee, C.; Lee, G. H.; Hone, J.; Heinz, T. F.; Shan, J. Tightly Bound Trions in Monolayer MoS<sub>2</sub>. *Nat. Mater.* **2012**, *12*, 207–211.

(34) Lin, Y.; Ling, X.; Yu, L.; Huang, S.; Hsu, A. L.; Lee, Y.-H.; Kong, J.; Dresselhaus, M. S.; Palacios, T. Dielectric Screening of Excitons and Trions in Single-Layer MoS<sub>2</sub>. *Nano Lett.* **2014**, *14*, 5569–5576.

(35) Krivosheeva, A. V.; Shaposhnikov, V. L.; Borisenko, V. E.; Lazzari, J.-L.; Waileong, C.; Guskova, J.; Tay, B. K. Theoretical Study of Defect Impact on Two-Dimensional MoS<sub>2</sub>. *J. Semicond.* **2015**, *36*, 122002.

(36) Lince, J. R.; Hilton, M. R.; Bommannavar, A. S. Oxygen Substitution in Sputter-Deposited MoS<sub>2</sub> Films Studied by Extended X-Ray Absorption Fine Structure, X-Ray Photoelectron Spectroscopy and X-Ray Diffraction. *Surf. Coat. Technol.* **1990**, *43–44*, 640–651.

(37) Zhao, B.; Shang, C.; Qi, N.; Chen, Z. Y.; Chen, Z. Q. Stability of Defects in Monolayer MoS<sub>2</sub> and Their Interaction with O<sub>2</sub> Molecule: A First-Principles Study. *Appl. Surf. Sci.* **2017**, *412*, 385–393.

(38) Fleischauer, P. D.; Lince, J. R. A Comparison of Oxidation and Oxygen Substitution in MoS<sub>2</sub> Solid Film Lubricants. *Tribol. Int.* **1999**, *32*, 627–636.

(39) Le, D.; Rawal, T. B.; Rahman, T. S. Single-Layer MoS<sub>2</sub> with Sulfur Vacancies: Structure and Catalytic Application. *J. Phys. Chem. C* **2014**, *118*, 5346–5351.

(40) Yin, Y.; Han, J.; Zhang, Y.; Zhang, X.; Xu, P.; Yuan, Q.; Samad, L.; Wang, X.; Wang, Y.; Zhang, Z.; et al. Contributions of Phase, Sulfur Vacancies, and Edges to the Hydrogen Evolution Reaction Catalytic Activity of Porous Molybdenum Disulfide Nanosheets. *J. Am. Chem. Soc.* **2016**, *138*, 7965–7972.

(41) Li, G.; Zhang, D.; Qiao, Q.; Yu, Y.; Peterson, D.; Zafar, A.; Kumar, R.; Curtarolo, S.; Hunte, F.; Shannon, S.; et al. All The Catalytic Active Sites of MoS<sub>2</sub> for Hydrogen Evolution. *J. Am. Chem. Soc.* **2016**, *138*, 16632–16638.

(42) Najmaei, S.; Liu, Z.; Zhou, W.; Zou, X.; Shi, G.; Lei, S.; Yakobson, B. I.; Idrobo, J.-C.; Ajayan, P. M.; Lou, J. Vapour Phase Growth and Grain Boundary Structure of Molybdenum Disulphide Atomic Layers. *Nat. Mater.* **2013**, *12*, 754–759.